

Molecularly Hybridized Conduction in DPP-Based Donor–Acceptor Copolymers toward High-Performance Iono-Electronics

Sanket Samal, Heejung Roh, Camille E. Cunin, Geon Gug Yang, and Aristide Gumyusenge*

Iono-electronics, that is, transducing devices able to translate ionic injection into electrical output, continue to demand a variety of mixed ionic–electronic conductors (MIECs). Though polar sidechains are widely used in designing novel polymer MIECs, it remains unclear to chemists how much balance is needed between the two antagonistic modes of transport (ion permeability and electronic charge transport) to yield high-performance materials. Here, the impact of molecularly hybridizing ion permeability and charge mobility in semiconducting polymers on their performance in electrochemical and synaptic transistors is investigated. A series of diketopyrrolopyrrole (DPP)-based copolymers are employed to demonstrate the multifunctionality attained by controlling the density of polar sidechains along the backbone. Notably, efficient electrochemical signal transduction and reliable synaptic plasticity are demonstrated via controlled ion insertion and retention. The newly designed DPP-based copolymers further demonstrate unprecedented thermal tolerance among organic mixed ionic–electronic conductors, a key property in the manufacturing of organic electronics.

neural networks (ANNs) would then be achievable toward energy efficiency, error-tolerance, high inter-wiring, and parallel processing and remembering of biological stimuli, to closely imitate the natural brain.^[7–9] On this front, organic mixed ionic–electronic conductors (OMIECs) are currently playing an integral role in advancing electronics able to reliably mimic and interface with biology.^[10–12] Owing to their ability to respond to ionic flux by changing their properties (conductance, color, modulus, or volume change),^[13–15] these materials are attractive for the realization of artificial synapses with high-accuracy signal transduction. Besides, these materials are attractive for their solution-processability, biocompatibility, and structural alterability.^[1,16,17]

1. Introduction


The field of bioelectronics continues to evolve toward large-area, body-compatible, and adaptive electronics.^[1–4] The next-generation electronics are aimed to be in more intimate contact with the biological circuitry to complement and/or replace physiological functions. For such integrations, these electronics must emulate natural sensing and computing capabilities. An intriguing task has thus become the emulation of synaptic functionalities in order to assist and/or mimic the brain.^[5,6] Owing to their mechanically soft nature coupled with tunable optoelectronic properties, organic materials are attractive for this application. With effective organic-based artificial synapses, artificial

Organic electrochemical transistors (OECTs) are the most widely studied device architecture for realizing artificial synaptic functionalities using organic materials.^[18] In such devices, a mixed ionic–electronic conductor is put in direct contact with an electrolyte, and its conductance state is tuned through the gate polarity which inserts or extracts ions in or out of the material bulk. Given that ionic species can be imbibed by the semiconductor bulk, the electrochemical modulation of the bulk becomes facile, making OECTs less power-hungry than conventional transistors. Most OECTs can be turned ON and OFF within a 2 V range making them great candidates for signal amplification at the biological interface.^[18] One of the major challenges in the field presently is the design and synthesis of semiconductors that can meet all stringent requirements for the practical demonstration of advanced bioelectronics.^[19,20]

The state-of-the-art materials in OECTs are commonly conjugated polymers bearing polar side groups or polymer-polyelectrolyte blends which can uptake electrolytic species and enable redox activity in the film bulk and achieve mixed ionic–electronic conduction.^[14] A prime and most studied example of such polymers is poly(3,4-ethylenedioxythiophene):poly(styrene sulfonate) (PEDOT:PSS), a commercially available colloidal suspension with excellent electronic and ionic conductivity. PEDOT:PSS has yielded high-performing OECTs, neuro-morphic devices, bioimaging devices, and neural probes.^[2,21–23] Despite its widespread use, however, this polymer system faces several fundamental challenges which have sparked further investigation on materials design for OECT materials.^[20]

S. Samal, H. Roh, C. E. Cunin, A. Gumyusenge
Massachusetts Institute of Technology
Department of Materials Science & Engineering
77 Massachusetts Ave, Cambridge, MA 02139, USA
E-mail: aristide@mit.edu

G. G. Yang
Korea Advanced Institute of Science & Technology (KAIST)
291 Daehak-ro, Yuseong-gu, Daejeon 34141, South Korea

 The ORCID identification number(s) for the author(s) of this article can be found under <https://doi.org/10.1002/smll.202207554>.

© 2023 The Authors. Small published by Wiley-VCH GmbH. This is an open access article under the terms of the Creative Commons Attribution License, which permits use, distribution and reproduction in any medium, provided the original work is properly cited.

DOI: 10.1002/smll.202207554

To name but a few challenges, i) PEDOT:PSS requires additive-heavy processing and post-deposition treatments which vary from laboratory to laboratory making replication a challenge.^[24,25] ii) PEDOT:PSS-based OECTs inherently operate in depletion mode, that is, the channel is intrinsically “ON” and an energy penalty must be paid to switch it “OFF”, which is not desirable for practical use.^[26] Additionally, iii) the “ON” current levels in PEDOT:PSS-based devices tend to be elevated and incompatible with biological environments; chemical modifications are often required to dilute down its conductivity for applications.^[25] The field has thus made substantial efforts to find alternative materials mainly employing sidechain engineering,^[27] copolymerization,^[20,28,29] and additive strategies.^[30] A recent notable candidate is poly(2-(3,3'-bis(2-(2-(2-methoxyethoxy)ethoxy)ethoxy)-[2,2'-bithiophen]-5-yl)thieno[3,2-b]thiophene), pg2T-TT, a p-type mixed conductor which, despite a few remaining challenges around stability, has shown outstanding performance in electrochemical devices, synaptic transistors, and sensing devices.^[9,26] Structurally, pg2T-TT depicts a model conjugated backbone flanked with polar sidechains for facile ion uptake and conductance modulation; several derivatives have thus been reported by varying the side chains and their distribution.^[31]

Despite recent efforts in designing high-performance mixed conductors, several challenges mainly related to operational stability remain: 1) the stellar polymer candidates are easily oxidized in ambient conditions which complicates reliable structure-property studies and leads to inconsistencies in reported figures of merit such as the threshold voltage and transconductance; 2) no polymer candidate has thus far shown the needed compatibility with back-end-of-line (BEOL) conditions (typically 300 °C baking steps) for large-area manufacturing and hardware integration; 3) the commonly studied homopolymers (e.g., pg2T-TT derivatives) are typically synthesized as low molecular weight chains resulting in easy dissolvability in electrolytes, low electronic mobility, poor long-term stability, as well as the abovementioned data replication issues. To propel the field of organic electronics forward, further molecular design efforts are needed to address these remaining challenges. Given the molecular tunability of conjugated polymers, there is, without a doubt, a platform to further improve their structures and yield next-generation organic conductors. On this end, we believe the challenge stems from the disconnect between disciplines where the chemists who design and synthesize the materials are not necessarily device experts. An application-guided systematic design of novel conductors involving both chemists and engineers would be a much more effective strategy to yield novel materials and improve performances.

In this work, to i) uncover the importance of balanced ionic-electronic conduction, ii) unravel the packing behavior between polar and non-polar units along polymer chains, and iii) investigate the contribution from both the ion and electron-transporting blocks to the bulk electrochemical activity, we designed a series of diketopyrrolopyrrole (DPP)-based copolymers and studied their solid-state properties, as well as their electrochemical response to ionic insertion. To attain effective mixed ionic-electronic conduction, we copolymerized a DPP acceptor unit with a glycol-functionalized thiophene-thiophene donor and interrogated the impact of increased density of the polar side chains

on the resulting performance in electrochemical devices. We found that this copolymerization strategy yields highly uniform, semicrystalline, and redox-active thin films. The distribution of glycol-functionalized units in thin films was then investigated to reveal that, with systematically balanced ionic-electronic conduction, donor-acceptor copolymers can efficiently uptake ions both in aqueous and non-aqueous electrolytes while retaining excellent electronic transport. Such balanced conduction was found to translate into high-performance electrochemical and synaptic transistors. More importantly, we showed that through systematic copolymerization, we can tune the volumetric capacitance while conserving electronic mobility and span a variety of performance parameters in electrochemical transistor devices. Finally, we explored the ability of DPP-based mixed conductors to sustain extreme temperatures, a property that is currently unattainable in OMIECs. The copolymers studied herein could retain their electrochemical properties after undergoing a baking step at 300 °C, demonstrating the first-of-its-kind BEOL-compatible organic mixed conductors. We show that structural tunability enabled by copolymerization in DPP-based polymers is a versatile approach for exploring the multifunctionality of OMIECs and that molecular fine-tuning enables the use of existing semiconductors toward advanced organic electronics.

2. Results and Discussion

To design ionic-electronic conductors with well-balanced conductivity, we chose to use a DPP acceptor core, one of the most studied building blocks in organic electronics owing to its intrinsic planarity and hence efficient charge delocalization, structural tunability, and facile synthesis, especially via coupling copolymerization.^[32] Besides yielding high-performance electronic devices, DPP-based polymers have been shown to provide tunability in their physical properties to address processability and stability challenges found in organic electronics.^[32–34] Particularly in OECT devices, DPP-based polymers have been employed when either flanked with polar sidechains (e.g., oligoethers) or copolymerized with donor blocks bearing polar groups to attain mixed ionic electronic conduction.^[29,35–37] To date, these systems are among the top performers in electrochemical devices.^[20,38] However, though DPP polymers continue to find use in electrochemical devices, from a molecular design viewpoint, increasing the ion uptake capabilities (maximizing the volumetric capacitance) has been the major focus. Little to no work has been done on systematically investigating how ion-friendly side groups can be appended onto the DPP backbone without greatly hampering its planarity and efficient stacking between adjacent chains. For instance, theoretical efforts by Khot et al. have suggested that, in order to maximize charge mobility and conductivity in OMIECs, optimal distribution between hydrophilic and hydrophobic sidechains should be targeted,^[39] but no experimental effort has yet to complement these predictions toward designing high performing mixed conductors, a property that has proved useful in other systems.^[11,40] In fact, in most reported DPP-based redox active copolymers, the polar groups are uncontrollably appended onto conjugated backbones and the electronic properties are often largely sacrificed.^[20,38]

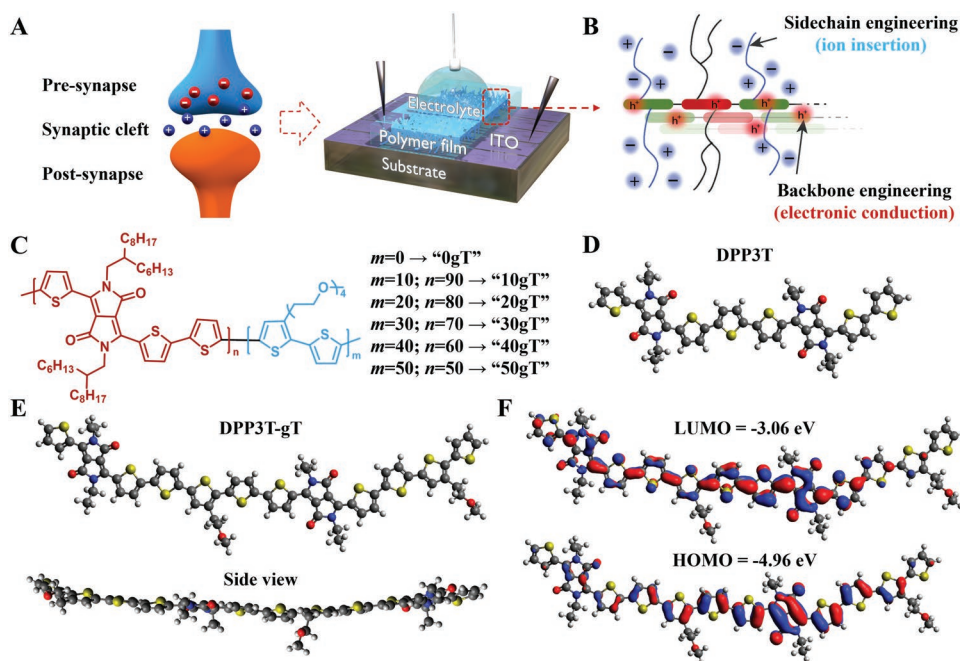


Figure 1. Hybridizing ionic and electronic conduction in DPP-based polymers. A) Illustration of a synaptic transistor and the use of organic mixed ionic–electronic conductors for electrochemical conductance modulation. B) General structure of polymer mixed conductors. C) Molecular structure of hybrid DPP copolymers for attaining mixed ionic–electronic conduction. D,E) Optimized geometries of the parent DPP and the hybridized copolymer, as well as the corresponding side view. F) Frontier molecular orbitals of the glycol functionalized copolymer using density functional theory (DFT) calculations (B3LYP/6-31+G(d)).

Here, we aimed to fully uncover the relationship between the polymer structure and electrochemical properties, by investigating i) the required balance between the highly planar and electronic conducting unit and the co-monomers bearing ion-friendly sidechains; ii) how the efficient stacking and the planar nature of DPP polymers can be retained in resulting redox-active copolymers; as well as iii) the impact of slowly increasing the density of polar groups on the physical properties of the polymer films. Our hypothesis is that if we can control the amount of oligoether groups along the backbone, we can establish the true relationship between mixed conduction and the polymer structure and find an optimal combination between ion permeability and electronic conduction (Figure 1A,B). We then designed and synthesized a series of DPP copolymers with varying densities of glycolated thiophene donor unit (ngT). The molecular structures are shown in Figure 1C, and monomer preparation and polymer synthesis are described extensively in the Supplementary Information.

We synthesized all the polymers through Stille coupling polymerization between the dibromo-pyrrolopyrrole monomers, dibromo-glycol-thiophene monomers, and trimethylstannyl-thiophene monomers. Starting with the fully alkylated donor-acceptor polymer poly[2,2'-(2,5-bis(2-hexadecyl)-3,6-dioxo-2,3,5,6-tetrahydropyrrolo[3,4-c]pyrrole-1,4-diyl)dithiophene]-5,5'-diyl-alt-thiophene-2,5-diyl] termed here PDPP3T-0gT. The percent ratio between the glycolated thiophene and alkylated DPP was then increased from 10% to 50% to yield the ngT series (0gT, 10gT, 20gT, 30gT, 40gT, and 50gT) as shown in Figure 1C. The feed ratios between the two dibromo monomers were controlled systematically to get the ngT series with the ratios

verified by ^1H NMR spectroscopy and presented in the Supporting Information (Figures S1–S6, Supporting Information). All polymers show excellent solubility in chloroform with concentrations as high as 20 mg mL^{-1} for further characterization. The molecular weight (M_n) and dispersity values (\mathcal{D}) of all the ngT polymers were extracted through gel permeation chromatography (GPC) and provided in the Supporting Information. The polymers were designed so that the glycolated thiophene is added sequentially without any direct contact with the DPP motif, which should afford retained crystallinity of the polymers with strong interchain interactions, while systematically opening the polymer bulk enough for enhanced ion infiltration. We hypothesize that this would affect the optoelectronic and solid-state properties of the copolymers and we aimed to relate such tunability to resulting device performances.

We first employed cyclic voltammetry (CV) to demonstrate that copolymerization has a minor effect on energy levels. The fully alkylated polymer (0gT) exhibits the highest occupied molecular orbital (HOMO) value of 5.25 eV, while the HOMO level rises to 5 eV for 50gT (Figure S7, Supporting Information). This trend in energy levels with increasing gT groups was also predicted by density functional theory (DFT) calculations (B3LYP/6-31+G(d)) for short oligomers of 0gT and 50gT, which resulted in the calculated HOMO energy levels of 5.1 and 4.96 eV, respectively (Figure 1D–F). At the same time, the DFT calculations revealed a highly delocalized lowest unoccupied molecular orbital (LUMO) along the entire π -conjugated system, even for 50gT, indicative of favorable charge carrier mobility (Figure 1F) as previously documented in DPP-based systems.^[41] The efficient charge transfer between the co-monomers was

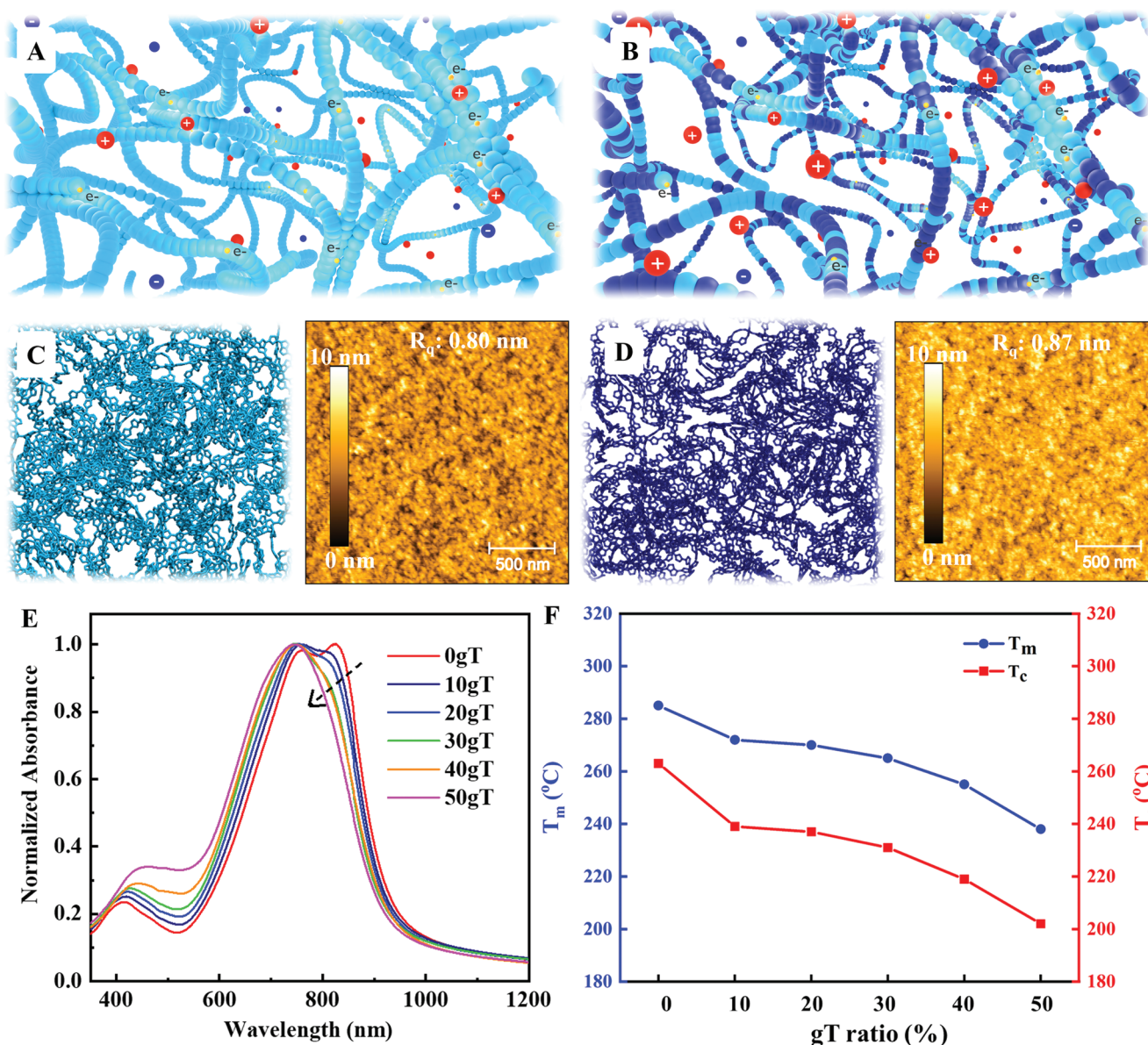


Figure 2. Solid state behavior in hybridized ionic-electronic conductors. Illustration of the proposed morphology of the studied DPP polymer A) before and B) after copolymerization. Snapshots from the molecular dynamics (MD) simulations and measured AFM height images from **0gT** (C) and **50gT** (D) polymer films. Sidechains are omitted from the MD images for clarity. E) Solid-state UV-vis absorption spectra from the **ngT** series. F) Measured melting and crystallization temperatures from the **ngT** copolymers.

also evidenced by solution UV-vis absorption spectra, which revealed characteristic a π - π^* transition delocalized between the donor and acceptor units, as well as the signature charge redistribution bands within DPP units (Figure S8, Supporting Information).^[42,43] That is, all copolymers showed a high energy transition (350–530 nm), which was associated with a bathochromic shift, and a lower energy absorption band (520–1000 nm), which was associated with a gradual hypsochromic shift with an increasing percentage of glycolated thiophene units and the overall D-A character conjugated backbone systematically decreases.

The effect of increasing the density of **gT** groups along the backbone was also revealed to impact the bulk optoelectronic

properties as we hypothesized for this series of copolymers (Figure 2A,B). We first confirmed the proposed morphology through molecular dynamics (MD) simulations. The calculations revealed that the alkylated DPP blocks can effectively pack with the thiophenes comonomers bearing the glycol chains (Figure 2C,D). This mixing between the two functionalized domains is highly desirable for efficient charge delocalization in polymer films.^[39] This simulated morphology was indeed confirmed using atomic force microscopy (AFM), which revealed no evidence of phase separation between the two building blocks. In fact, all polymers yield highly uniform and smooth thin films indicative of efficient co-existence between the “ionic” and “electronic” units (Figure 2C,D and Figure S9,

Supporting Information). This intermixing of the glycol functionalized units with the more hydrophobic regions of the polymer further showed to lower the overall surface energy of resulting films as the **ngT** percent increased (Figure S10, Supporting Information). Low surface energy is targeted here for the use of these polymers in electrolyte-gated transistor devices where the semiconducting polymer must come in direct contact with different electrolytes. The copolymerization strategy thus proved to be a viable route for tuning the polymer–electrolyte compatibility which will be further discussed in later sections.

To probe the effect of copolymerization on overall chain behavior at the molecular level, we first scanned the UV–vis absorption of the **ngT** series. The absorption spectra from annealed thin films revealed that, within the lower energy absorption band, concomitant with an overall blueshift, the intensity of the signature 0-0 vibronic peak associated with inter-chain stacking exhibited a hypochromic shift from **0gT** to **50gT** (Figure 2E). This indicates that as the amount of glycolated-thiophenes increases, there is less chain-chain aggregation. This behavior is of great interest for ion insertion, particularly in electrochemical devices. The copolymerization approach thus showed to enable gradual tuning of the aggregation behavior of mixed conductors through the controlled density of polar groups, a feature which is not readily attainable in homopolymers or polyelectrolytes.^[44,45] This lowered aggregation could further be confirmed by grazing incidence X-ray diffraction (GIXD) patterns obtained from the annealed thin films of the **ngT** polymers. All polymers show weakened diffraction intensities in comparison to analogous DPP-based polymers (Figure S11, Supporting Information).^[46–48] As a result of this molecular level de-aggregation, the **ngT** series shows softening upon the increasing amount of glycol groups in the bulk as evidenced by their dynamic scanning calorimetry (DSC) profiles shown in Figure 2F and Figures S12 and S13, Supporting Information. Both the melting and the crystallization temperatures (T_c and T_m) showed to decrease by nearly 50 °C as the **gT** percent increases from 0% to 50%, indicative of overall softening of the polymer bulk without sacrificing the overall thermal stability limit. Conventionally, DPP-based conjugated polymers are rigid and thus not suitable for facile ion transport. The copolymerization approach we report reveals to be an effective method to soften such systems and endow them with further properties that are needed for mixed conduction.

As hinted in previous sections, a key feature that makes OMIEC polymers highly multifunctional and attractive for a variety of applications is their ability to uptake ions and modulate their conductance.^[13,14] Ideally, such modulation is achieved under a variety of electrolytic environments. In the case of the **ngT** series studied herein, since we started with highly hydrophobic parent building blocks, we were intrigued by how systematically tethering glycol sidechains onto the backbone would affect the electrochemical response of resulting copolymers. We hypothesized that engineering different degrees of ionic uptake and retention would find relevance in a variety of applications, that is, different device operations might require different levels of ion permeability and retention. It would be of paramount importance if such properties could be tuned chemically and solve the one-material-fits-all approach that currently dominates the field of organic electronics. To probe the redox activity of

the **ngT** polymers, we carried out CV and spectro-electrochemical measurements in both aqueous (here 0.1 M LiPF₆) and non-aqueous (1-ethyl-3-methylimidazolium bis(trifluoromethylsulfonate)imide, EMIM TFSI) electrolytes. **Figure 3A** shows the voltammograms obtained in LiPF₆ with varying amounts of glycol groups. With a higher **ngT** percentage, we found that the redox activity of the polymers was greatly improved. The measured current density and hence the areal capacity showed to increase gradually due to enhanced ionic insertion into the polymer films with a higher density of the polar groups. This enhanced ionic uptake could also be supported by the above-discussed tunable surface energy in **ngT** thin films. Concomitantly, as shown in **Figure 3B**, the corresponding oxidation, as well as the onset potentials, showed to shift to lower values as the density of glycol groups increases and the surface energy decreases. Furthermore, a similar trend was observed using EMIM TFSI as the electrolyte (**Figure 3G,H**) showing that the designed **ngT** polymers are highly versatile in terms of electrolyte choice, which is attractive for designing electronic devices. This redox activity was further found to be highly reversible and stable, especially at high **gT** content (**Figure S14**, Supporting Information).

To accurately relate the observed oxidation and reduction properties to the insertion of ions into the film bulk, we scanned the UV, vis, and near-infrared (NIR) absorption behavior of the polymer films at different potentials during the electrochemical cycling. **Figures 3C,D** show the absorption spectra from **0gT** and **50gT** films, respectively, in 0.1 M LiPF₆. In agreement with the CV results, we found that the copolymer films uptake varying amounts of ions as the working potentials increase and become bleached indicative of volumetric oxidation. The extracted peak intensities in select ranges (750 nm in the visible range and 1100 nm in NIR) reveal that the electrolyte is indeed able to permeate through the film bulk, oxidizing the semiconducting polymer chains, thus depleting the absorption in the visible range at the expense of the then formed polarons and bipolarons which absorb much higher wavelengths.^[37,49] With increasing **gT** percent, the bleaching behavior and polaron/bipolaron formation showed to require much lower applied voltages (**Figure 3C–F**), revealing that as anticipated, the glycol-functionalized copolymers uptake hydrated ionic species much easier than the parent DPP films. In agreement with the CV results discussed above, efficient bulk modulation was also observed when using a neat ionic liquid (EMIM TFSI) as the electrolyte (**Figure 3I–L**). In fact, with as low as 0.4 V applied onto the working electrode, **50gT** shows significant bleach (depleted absorption intensity in the visible region) while the parent **0gT** required twice as much voltage to show any change in its absorption spectrum. With such a tunable degree of ion insertion to modulate the optoelectronic behavior of the **ngT** copolymers, we expect this series to find a multitude of applications using electrochemical response in various operation environments. Most importantly, the ability to achieve these behaviors through molecular tuning is highly attractive as this copolymerization strategy can be expanded onto other building blocks and sidechains to generate novel OMIECs.

The major hard-to-crack trade-off in designing OMIECs is retaining high charge carrier mobilities in capacitive and ion-permeable systems. To yield high-performance electrolyte-gated

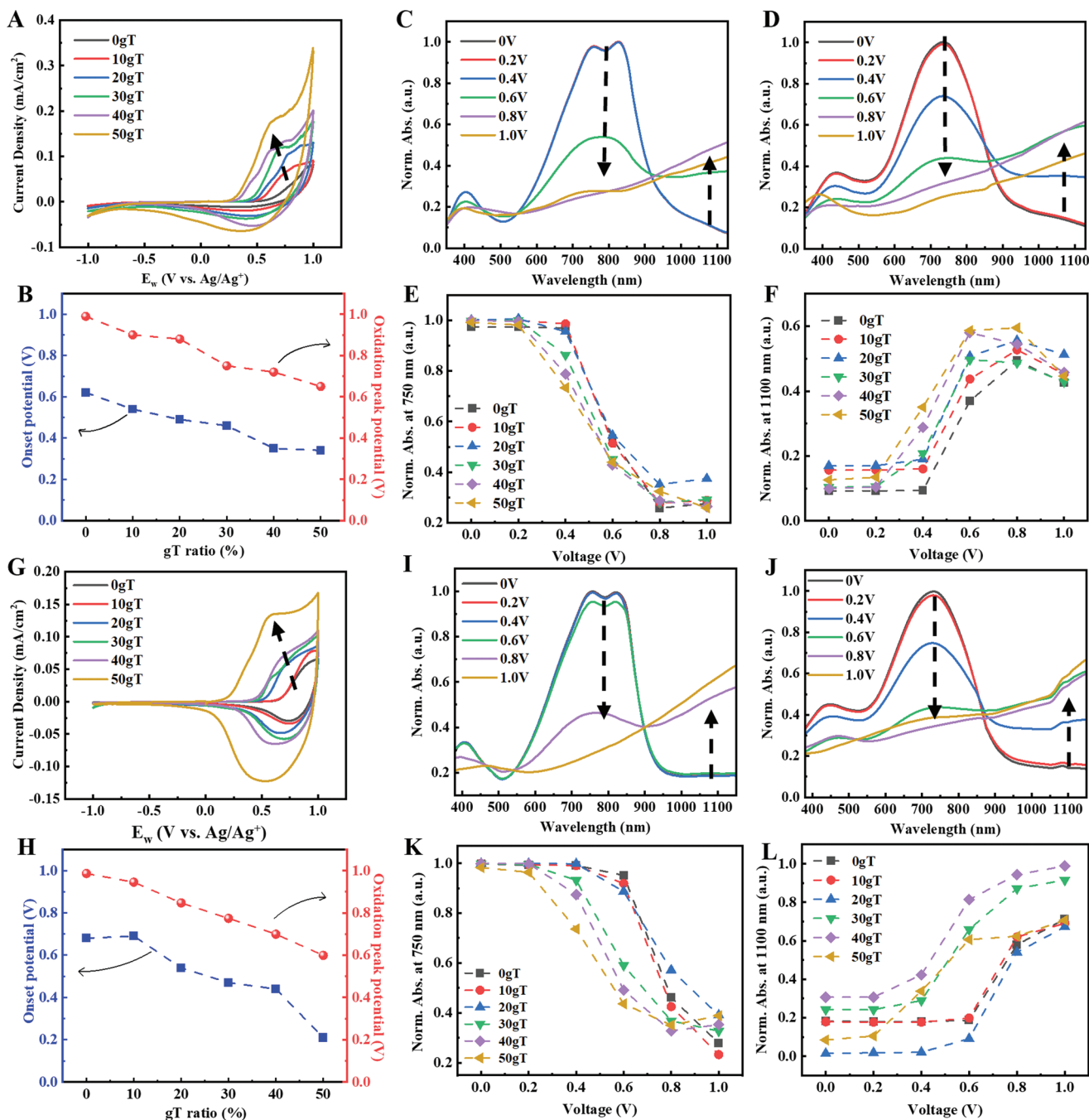


Figure 3. Redox-activity tunability in DPP-ngT series. A) Cyclic voltammograms in aqueous 0.1 M LiPF₆, and B) corresponding onset potential and oxidation potentials. C, D) Spectro-electrochemical behaviors of 0gT and 50gT, respectively, in 0.1 M LiPF₆. E, F) Extracted absorption intensity at 750 and 1100 nm, respectively. G) Cyclic voltammograms in EMIM TFSI, and H) corresponding onset potential and oxidation potentials. I, J) Spectro-electrochemical behaviors of 0gT and 50gT, respectively, in EMIM TFSI. K, L) Extracted absorption intensity at 750 and 1100 nm, respectively.

transistor devices, for instance, the above-discussed electrochemical properties must be complemented with high electronic mobility. To probe the effect of the increased density of polar sidechains on the electronic performance of the ngT copolymers, we first fabricated field-effect transistors (FETs) and characterized the corresponding charge carrier properties. Here, we are interested in establishing how “electronic” a mixed conductor needs to be in order to perform efficiently

in electrochemically gated devices. Typically, when designing OMIECs, most works focus on increasing the capacitive properties of the polymer through large densities of polar sidechains, and less emphasis is placed on retaining the intrinsic charge mobility.^[50–52] As such, it is not readily intuitive to select the amount of ion-transporting side groups needed for various ionoelectronic applications. Though we are intentionally appending polar groups onto conjugated backbones which would lead to

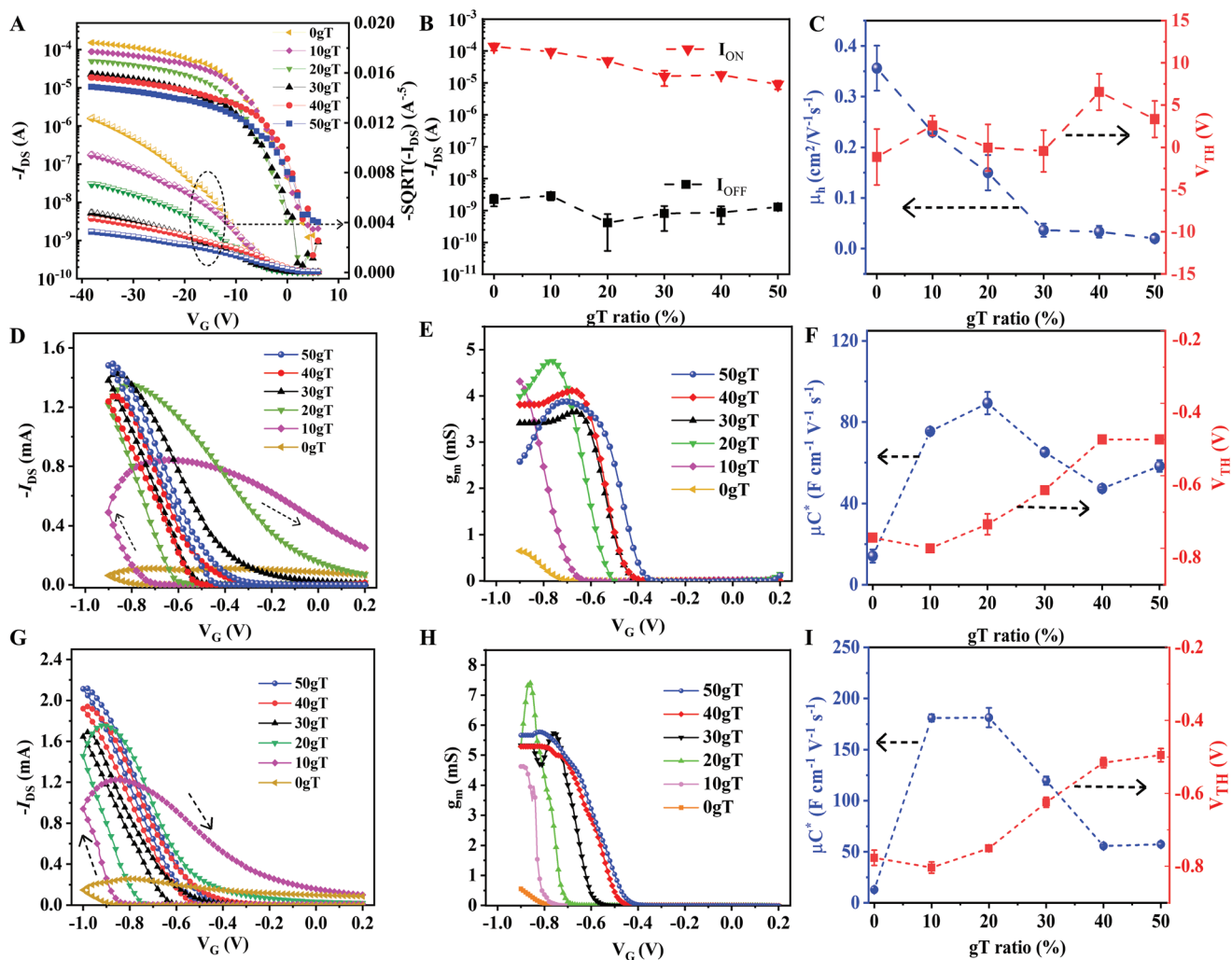


Figure 4. Mixed ionic electronic conduction in molecularly hybridized conductors. A–C) Characteristic electronic performance from FET devices based on **ngT** polymer films. Transfer characteristic and extracted performance parameters from **ngT**-based OECT devices in aqueous (D–F) and non-aqueous (G–I) electrolytes.

lowered charge carrier mobility, we hypothesize that systematic balancing between the DPP unit and the glycol-bearing thiophene, as well as the strategic placement of the oxygen far from the backbone, we can retain excellent charge transport in solid state devices. Most importantly, by molecularly separating the electron-favoring units from the ion-solvating comonomers, we can systematically relate the density of polar groups present along the backbone to the resulting electronic performance and its contribution to the electrochemical performance. **Figure 4A** shows the characteristic transfer curves obtained from the **ngT** series and the corresponding characteristic output curves are shown in Figure S15, Supporting Information. As we expected, the polar sidechains which would act as charge trapping sites in FETs, indeed led to a gradual decline in the “ON” current, as well as the charge carrier mobility with increasing **gT** percentage. However, even with as high as 50% of **gT** in the backbone, the OFET devices still retained excellent hole mobility as high as $0.01 \text{ cm}^2 \text{ Vs}^{-1}$ and I_{ON}/I_{OFF} higher than 10^5 (Figure 4B,C). More impressively, with as high as 20% of

gT groups along the backbone, the resulting transistor devices exhibit mobilities as high as $0.15 \text{ cm}^2 \text{ Vs}^{-1}$ with relatively low threshold voltages ($V_{th} \approx -5 \text{ V}$) (Figure 4C). Such efficient charge carrier transport, once coupled with capacitive properties in mixed conductors, is expected to contribute to high-performance iono-electronic devices.

To probe the mixed ionic–electronic conduction of **ngT** series, we then characterized their performance in OECT devices using both aqueous (LiPF_6) and non-aqueous (EMIM TFSI) electrolytes. In such device configuration, we aimed to probe the ability of the copolymers to combine ionic uptake, thus conductance modulation, with electronic charge transport. Figure 4D shows the measured transfer currents for all **ngT** polymers using aqueous 0.1 M LiPF_6 as the electrolyte and Figure 4E shows the extracted transconductance values (g_m). Through electrochemical gating, we first found that the higher the density of **gT** groups, the higher the device current when similar dimensions are employed ($L = 50 \text{ }\mu\text{m}$, $W = 4.5 \text{ mm}$). At the same time, the hysteresis behavior of the polymer-based

devices showed to greatly improve with an increasing percentage of **gT** groups. That is, with a higher percentage of polar groups we observed a greater overlap (low hysteresis) in measured currents when the gate voltage was swept forward and backward. The threshold voltage also showed to shift to lower values with an increasing percentage of **gT** groups (Figure 4F), indicative of more facile ionic insertion into the film bulk with more polar groups present in great agreement with the electrochemical behaviors discussed above. With a controllable density of polar groups throughout the film bulk, we could thus control the operation voltage and response speed. More intriguingly, the μC^* product, a measure of mixed ionic–electronic conduction in OMIECs, showed to be optimal in the case of **20 gT** (Figure 4F). With the current device dimensions, a μC^* of $95 \text{ F cm}^{-1} \text{ V}^{-1} \text{ s}^{-1}$ was calculated in LiPF_6 as the electrolyte. Other relevant device parameters are also summarized in Table S1, Supporting Information.

To mirror these electrochemical measurements in non-aqueous conditions, we further employed a neat solution of EMIM TFSI and tested the OECT device performance. Similar to the behavior observed in aqueous conditions, measured current showed to increase with the amount of glycolated thiophenes present (Figure 4G,H). The representative transfer and output curves are shown in Figure S16, Supporting Information. Like the case of LiPF_6 , the extracted g_m and hence μC^* values showed to be optimal with 20% of the **gT** units present. In fact, g_m values as high as 7.5 mS and μC^* of $176 \text{ F cm}^{-1} \text{ V}^{-1} \text{ s}^{-1}$ (device dimensions: $L = 50 \text{ }\mu\text{m}$, $W = 5 \text{ mm}$) which are among the best among DPP-based OMIECs, could be measured using the **20gT** polymer. It was thus evident that to optimize the mixed conduction parameters in these polymers, it is important to consider both the ion permeability of the film bulk (through increased density of polar groups) and high charge carrier mobility. With careful selection of sidechains,^[51,53,54] donor–acceptor units,^[49,28] electrolyte choice,^[55] as well as the device dimension optimization,^[56] we expect these figures of merits to be further improved and the copolymerization strategy to be a versatile method for other material makers to meet various needs in organic electronics. This ability to tune the device metrics from a materials design approach is crucial in designing next-generation OMIECs, a field where multifunctional materials are becoming common and single-material systems can be employed for different functions.^[13] In the case of the **ngT** series reported here, not only can we control the operation voltage here but also the charge retention times making these materials suitable for both signal transduction and charge retention.

Given that we can tune the ability of these DPP-based polymers to retain the electrochemically injected charges, we set out to investigate their performance as channel materials for ion-based synaptic plasticity. Ionic memory has recently garnered a great deal of attention, especially in neuromorphic computing.^[9,57,58] Not only does the use of ion insertion in memory devices emulate the mechanism found in the biological memory system, but it has also been shown to be energy efficient, deployable to various classes of materials, and promising toward high-fidelity ANNs.^[9,57] To test the utility of the **ngT** polymers in advanced ionic-electronics, we fabricated electrochemical neuromorphic devices (ENDs) and characterized the impact of tuned **gT** percentage on the electrochemical

synaptic plasticity. In these devices, a gate electrode is used to mimic a pre-synaptic neuron and send electrical pulses to tune the injection and extraction of ions from the electrolyte to the semiconducting channel. The conductance changes induced in the channel are thus recorded as the current flowing between the source and drain contacts, analogous to the post-synaptic current, as illustrated in Figure 5A. For comparison, we selected two representative copolymers, **20gT** and **50gT**, and tested their performance in ENDs using 0.1 M LiPF_6 aqueous solution as an electrolyte.

First, we tested the spike number-dependent plasticity (SNDP) on the ENDs using **20gT** and **50gT**. To do so, we applied a series of -1 V pulses at the gate electrode with a pulse width of 40 ms and monitored the current flowing between the source and drain. As shown in Figure 5A,B, both **20gT** and **50gT** demonstrate a significant increase in the post-synaptic current upon spiking. The measured postsynaptic current also depends greatly on the number of pulses applied to the gate electrode. This behavior is analogous to the learning mechanism found in biological neurons, where cells that fire more frequently, exhibit higher synaptic weights, a property that is crucial for learning and remembering.^[59,60] Furthermore, we characterized the ability of **ngT** polymers to realize long-term potentiation (LTP) and depression (LTD), which are important metrics for the reliable deployment of artificial synapses for tasks such as image recognition. The synthetic synapses must be able to train accurately, which requires a series of writing and erasing cycles. When we applied 100 negative pulses (40 ms wide) followed by 100 positive pulses, both **20gT** and **50gT**-based devices show excellent modulation and erasing in the postsynaptic current (Figure 5C,D). Though both polymers exhibit modest linearity in the current responses, the ENDs achieve reversible learning, which is attractive in neuromorphic computing. **20gT**-based devices could achieve a dynamic range as high as $7\times$, while **50gT** devices could reach an analog switching range as high as $200\times$. Such large modulation between the high-resistance state and the low-resistance state is desirable for high-accuracy neural simulations. We attribute the larger dynamic range in **50gT** devices to the ability of the polymer bulk to uptake more ionic species and modulate the conductance, in agreement with the spectro-electrochemical results. Despite the modest endurance found in our polymers when LiPF_6 is used as an electrolyte (Figure S17, Supporting Information), the **ngT** series shows extremely promising behaviors toward the development of high-performance organic neuromorphic devices. With further optimization in electrolyte choices, devices miniaturization, and pulsing schemes, we believe the co-polymerization approach that we are reporting here can yield high-performance and high-field artificial synapses. The structural tunability we report enables further optimization and provides a deeper understanding of the relationships between polymer structure and device learning behavior.

One of the major shortcomings in organic semiconductors, which have been studied for neuromorphic computing to date, is their thermal intolerance which renders them incompatible with chip manufacturing. Typically, the semiconducting channels must undergo baking steps at the BEOL, which temperatures as high as $300 \text{ }^\circ\text{C}$.^[61] Currently, no polymer system has been shown to sustain such conditions, posing a challenge for

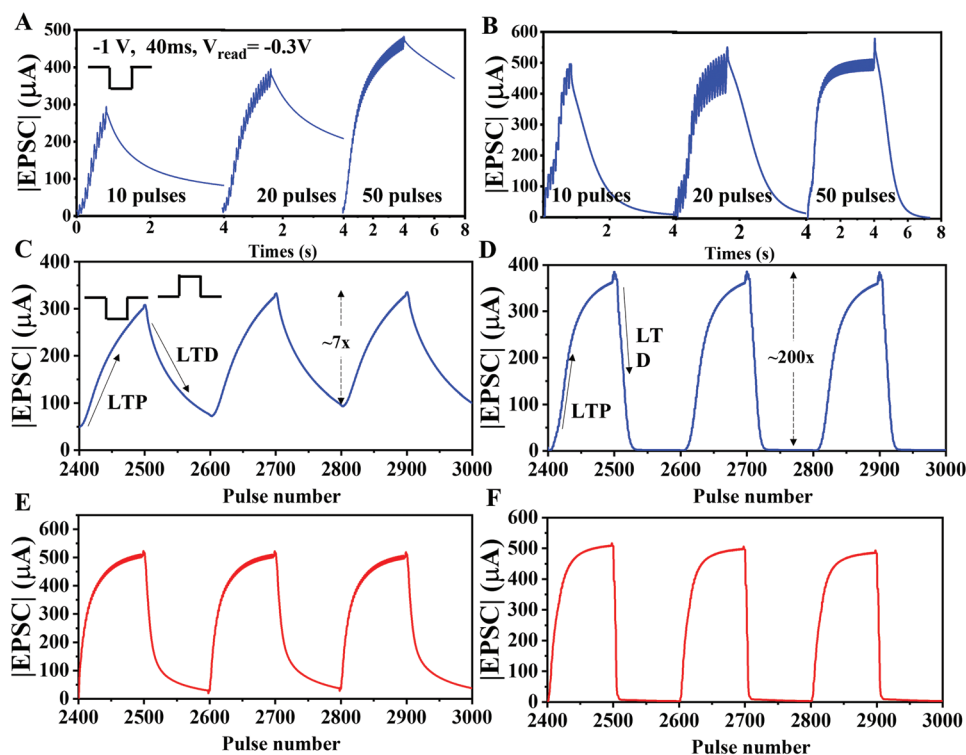


Figure 5. Ion-controlled synaptic behavior in DPP-based copolymers. A,B) Spike-number-dependent plasticity of transistors based on 20gT and 50gT films, respectively. C,D) Corresponding post-synaptic current responses to a series of write/erase pulses. Both E) 20gT and F) 50gT showed dynamic response and also showed excellent endurance after the semiconducting layer was baked to 300 °C.

integrating organic-based synaptic devices in advanced circuits. The bottleneck stems from the fact that to enable ion insertion, polar and bulky sidechains are employed. This strategy renders most mixed ionic–electronic conductors (MIECs) rather soft and thermally intolerant. In the case of PEDOT:PSS, thermal treatment deteriorates the microstructure with the films and decouples the two blend components; its thermal stability window is limited to around 100 °C despite being the most widely used semiconductor in organic devices.^[44,62] Since DPP-based polymers have shown to be thermally tolerant, we investigated the ability of our OECTs and ENDS to sustain extreme heat treatments. From the DSC profiles discussed above, we expected the ngT polymers to melt and recrystallize between 200 and 280 °C without deteriorating. We thus tested the transistor device performance after baking at 300 °C. Figure S18, Supporting Information, shows the OECT transfer curves from 20gT and 50gT before and after baking, respectively. Impressively, the thermal treatment showed to slightly enhance the ionic uptake by the polymer film and hence, the high source-drain current. We attributed this enhancement in the device response to the softening of the polymer films, and thus, more facile insertion of ions, however, further investigations to probe any potential structural changes within the films are warranted. Furthermore, the synaptic devices retained excellent responses in the post-synaptic currents. Figures 5E,F show the LTP and LTD responses after baking from 20gT and 50gT, respectively, indicative of excellent thermal stability of the gT series. In the case of 20gT, the switching dynamic range showed further improvement after baking (Figure 5E) likely due to the above-

discussed additional softening of the polymer film. We expect the thermal tolerance found in DPP-based OMIECs to enable further device designs, especially in circuits that require harsh baking steps. Besides, such thermal tolerance is envisioned to enable stable operation of resulting electronics in harsh environments.

3. Conclusions

The current work aimed to establish the relationship between the density of polar groups and the iono-electronic behavior in conjugated polymers. We use a DPP-based series to demonstrate that copolymerization is a facile route to tune the functionality of semiconducting polymers. Most importantly, we show that molecularly controlling the amount of glycol sidechains along the polymer chains is crucial for the optimization of resulting device performance. We show that when targeting electrolyte-gated transistors, it is important to retain high electronic transport, which is achievable by balancing the density of polar and non-polar segments of the polymer chain. This molecular-level hybridization contrasts with common strategies in the literature where volumetric capacitance is given higher priority. By controllably engineering the ionic uptake capabilities and electrolyte compatibility of conjugated polymers at the molecular level, we show that we can engineer novel MIECs and demonstrate multi-functional channel materials. Since different device operations require different levels of ion permeability and retention, we show that such properties can be tuned

chemically and solve the one-material-fits-all bottleneck that currently obstructs the field of organic electronics. The DPP-based ngT series studied here also exhibited unprecedented thermal tolerance, a promising step toward large-area device manufacturing and long-term operational stability.

4. Experimental Section

Materials: All conjugated polymers were synthesized following previous reports on DPP-based polymerization.^[47,48] The copolymerization is described in greater detail in Supporting Information. Semiconducting films were obtained by spin coating chloroform solutions followed by annealing in an inert environment. The electrolytes (LiPF₆ and EMIM TFSI) were purchased from Sigma Aldrich. Pre-patterned ITO substrates ($W = 5$ mm and $L = 50$ μ m) were purchased from Oscilla.

Morphological Studies: UV-vis absorption spectra were obtained using a Perkin Elmer 1050 UV-vis-NIR spectrophotometer. AFM images were taken using a Bruker Dimension Icon XR SPM and processed with Gwyddion Software. GIXDGIWAXS measurements were performed using a SAXSLAB Ganesha System, which uses a Rigaku 002 X-ray source and the data were processed using OriginLab Software.

Density Function Theory Calculations and Molecular Dynamics Simulations: DFT calculations were performed on the repeating units for **OgT** and **50gT** and the structures were optimized by using the B3LYP/6-31+G(d) level of theory in Gaussian 16. The input files and the output images of the molecules were generated using Avogadro molecular editor. All the MD calculations were done using LAMMPS molecular dynamics simulator.^[39] After the polymer chains were generated with ten repeating units, they were uploaded to Automated Topology Builder (ATB) and Repository (Version 3.0), to get the necessary topology files for MD calculations. These topology files were built using the GROMOS_54A7 force field and were downloaded directly from the ATB Repository. Using these topology files and force field files, a 3D simulation box of 300 Å was created with periodic boundary conditions and was packed with 64 chains of the polymer using a moltemplate. Each chain of the polymer was then permitted to relax within the MD simulation for 1 ns in isolation at 0 K in a vacuum using the LAMMPS suite, according to the intramolecular components of the GROMOS_54A7 force field. Then each chain was again permitted to relax within the MD simulation for 1 ns in isolation at 300 K using the same LAMMPS suite mimicking their behavior in solution. After that, this large simulation volume was compressed over a period of 1 ns at 300 K until the correct density was achieved, hence mimicking the spin coating of the solution into a thin film. Then the pressure was equilibrated to atmospheric pressure at constant volume and temperature, with timesteps of 1 fs, using the LAMMPS suite. Finally, further simulations were carried out to mimic annealing conditions, where the temperature was first increased from 300 to 400 K over a 1 ns period, then the annealed chains were again equilibrated to 300 K over a further period of 1 ns, before equilibrating at 300 K and atmospheric pressure for a total of 4 ns with timesteps of 0.5 fs.

Transistor Devices Fabrication: OFET devices were fabricated onto a heavily n-doped Si substrate with a 300 nm SiO₂ (capacitance of 11 nF cm⁻²) dielectric layer and Au source and drain electrodes ($W = 1500$ μ m and $L = 80$ μ m). Cleaned substrates were first modified with octadecyltrichlorosilane (OTS) following previous reports,^[63] and polymer films were spin-coated (2000 rpm, 40 s). OECT devices were fabricated by spin coating (900 rpm, 30 s) the polymer solutions onto cleaned and pre-patterned ITO substrates ($L = 50$ μ m, $W = 5$ mm). All polymer films were annealed at 120 °C for 30 min inside an N₂ glovebox and allowed to cool to ambient prior to measurements. For transistor devices studied after baking, OECTs were fabricated as described above and the devices were heated up to 300 °C inside an N₂ glovebox for 30 min and allowed to cool to room temperature before casting corresponding electrolytes and performing electrical measurements.

Electrochemical Characterization: CV measurements were carried out using a conventional 3-electrode setup with ngT films coated onto ITO as the working electrode, and a Pt spiral wire as the counter electrode, versus an Ag/AgCl reference. The electrochemical cell was purged with N₂ for a minimum of 30 min before the measurement. The spectroelectrochemical absorption responses were then collected using a Perkin Elmer 1050 UV-vis-NIR spectrophotometer in combination with SP-300 Potentiostat (Biologic).

Electrical Measurements: Electrical characterizations and pulsed measurements were carried out using a Keithley 4200 analyzer in an ambient environment. The pulsed measurements were programmed using an ultra-fast pulse measure unit coupled with a remote pre-amplified module. OFET performances were obtained by applying a gate bias from -40 to 6 V, with the potential gradient between the source and drain contacts kept at -40 V. The field-effect mobility was calculated in the saturation regime. For OECTs, the gate voltage was applied from -0.8 to 0.2 V and the source-drain voltage was set to -0.6 V (unless otherwise indicated). The volumetric capacitance (C^*) for each polymer was obtained using cyclic voltammetry in respective electrolytes,^[64] and a 4.5 mm-wide electrochemical cell was used to contain the liquid electrolytes during the measurements.

Supporting Information

Supporting Information is available from the Wiley Online Library or from the author.

Acknowledgements

S.S., H.R., and C.C. contributed equally to this work. A.G. and S.S. thank Prof. Barry Thompson for the molecular weight measurements and insightful discussion. G.Y. acknowledges support from Prof. Sang Ouk Kim and the Korea Advanced Institute of Science & Technology (KAIST). A.G. and C.C. acknowledge support from the K. Lisa Yang Brain-Body Center at the Massachusetts Institute of Technology (MIT).

Conflict of Interest

The authors declare no conflict of interest.

Data Availability Statement

The data that support the findings of this study are available in the supplementary material of this article.

Keywords

artificial synapses, iono-electronics, mixed conductors, organic, polymers, transistors

Received: December 3, 2022

Revised: January 17, 2023

Published online: February 3, 2023

- [1] T. Someya, Z. Bao, G. G. Malliaras, *Nature* **2016**, 540, 379.
- [2] I. B. Dimov, M. Moser, G. G. Malliaras, I. McCulloch, *Chem. Rev.* **2022**, 122, 4356.
- [3] H. Yuk, B. Lu, X. Zhao, *Chem. Soc. Rev.* **2019**, 48, 1642.

- [4] A. Canales, X. Jia, U. P. Froriep, R. A. Koppes, C. M. Tringides, J. Selvidge, C. Lu, C. Hou, L. Wei, Y. Fink, P. Anikeeva, *Nat. Biotechnol.* **2015**, *33*, 277.
- [5] Y. Kim, A. Chortos, W. Xu, Y. Liu, J. Y. Oh, D. Son, J. Kang, A. M. Foudeh, C. Zhu, Y. Lee, S. Niu, J. Liu, R. Pfattner, Z. Bao, T. W. Lee, *Science* **2018**, *360*, 998.
- [6] S. Dai, Y. Dai, Z. Zhao, F. Xia, Y. Li, Y. Liu, P. Cheng, J. Strzalka, S. Li, N. Li, Q. Su, S. Wai, W. Liu, C. Zhang, R. Zhao, J. J. Yang, R. Stevens, J. Xu, J. Huang, S. Wang, *Matter* **2022**, *5*, 3375.
- [7] I. Krauhaussen, D. A. Koutsouras, A. Melianas, S. T. Keene, K. Lieberth, H. Ledanseur, R. Sheelamanthula, A. Giovannitti, F. Torricelli, I. McCulloch, P. W. M. Blom, A. Salleo, Y. van de Burgt, P. Gkoupidenis, *Sci. Adv.* **2022**, *7*, eabl5068.
- [8] Y. van de Burgt, A. Melianas, S. T. Keene, G. Malliaras, A. Salleo, *Nat. Electron.* **2018**, *1*, 386.
- [9] E. J. Fuller, S. T. Keene, A. Melianas, Z. Wang, S. Agarwal, Y. Li, Y. Tuchman, C. D. James, M. J. Marinella, J. J. Yang, A. Salleo, A. A. Talin, *Science* **2019**, *364*, 570.
- [10] S. Inal, G. G. Malliaras, J. Rivnay, *Nat. Commun.* **2017**, *8*, 1767.
- [11] A. Savva, R. Hallani, C. Cendra, J. Surgailis, T. C. Hidalgo, S. Wustoni, R. Sheelamanthula, X. Chen, M. Kirkus, A. Giovannitti, A. Salleo, I. McCulloch, S. Inal, *Adv. Funct. Mater.* **2020**, *30*, 1907657.
- [12] D. T. Simon, E. O. Gabrielsson, K. Tybrandt, M. Berggren, *Chem. Rev.* **2016**, *116*, 13009.
- [13] S. T. M. Tan, A. Gumyusenge, T. J. Quill, G. S. LeCroy, G. E. Bonacchini, I. Denti, A. Salleo, *Adv. Mater.* **2022**, *34*, 2110406.
- [14] B. D. Paulsen, K. Tybrandt, E. Stavrinidou, J. Rivnay, *Nat. Mater.* **2020**, *19*, 13.
- [15] L. Q. Flagg, C. G. Bischak, J. W. Onorato, R. B. Rashid, C. K. Luscombe, D. S. Ginger, *J. Am. Chem. Soc.* **2019**, *141*, 4345.
- [16] A. Chortos, J. Liu, Z. Bao, *Nat. Mater.* **2016**, *15*, 937.
- [17] P. A. Ersman, R. Lassnig, J. Strandberg, D. Tu, V. Keshmiri, R. Forchheimer, S. Fabiano, G. Gustafsson, M. Berggren, *Nat. Commun.* **2019**, *10*, 5053.
- [18] J. Rivnay, S. Inal, A. Salleo, R. M. Owens, M. Berggren, G. G. Malliaras, *Nat. Rev. Mater.* **2018**, *3*, 17086.
- [19] N. A. Kukhta, A. Marks, C. K. Luscombe, *Chem. Rev.* **2022**, *122*, 4325.
- [20] P. Li, T. Lei, *J. Polym. Sci.* **2022**, *60*, 377.
- [21] C. Wang, X. Chen, L. Wang, M. Makihata, H.-C. Liu, T. Zhou, X. Zhao, *Science* **2022**, *377*, 517.
- [22] S. T. Keene, C. Lubrano, S. Kazemzadeh, A. Melianas, Y. Tuchman, G. Polino, P. Scognamiglio, L. Cinà, A. Salleo, Y. van de Burgt, F. Santoro, *Nat. Mater.* **2020**, *19*, 969.
- [23] E. Juzekaeva, A. Nasretdinov, S. Battistoni, T. Berzina, S. Iannotta, R. Khazipov, V. Erokhin, M. Mukhtarov, *Adv. Mater. Technol.* **2019**, *4*, 1800350.
- [24] S. T. Keene, T. P. A. van der Pol, D. Zakhidov, C. H. L. Weijtens, R. A. Janssen, A. Salleo, Y. van de Burgt, *Adv. Mater.* **2020**, *32*, 2000270.
- [25] S. T. Keene, W. Michaels, A. Melianas, T. J. Quill, E. J. Fuller, A. Giovannitti, I. McCulloch, A. A. Talin, C. J. Tassone, J. Qin, A. Troisi, A. Salleo, *J. Am. Chem. Soc.* **2022**, *144*, 10368.
- [26] A. Giovannitti, D.-T. Sbircea, S. Inal, C. B. Nielsen, E. Bandiello, D. A. Hanifi, M. Sessolo, G. G. Malliaras, I. McCulloch, J. Rivnay, *Proc. Natl. Acad. Sci. U. S. A.* **2016**, *113*, 12017.
- [27] J. W. Onorato, Z. Wang, Y. Sun, C. Nowak, L. Q. Flagg, R. Li, B. X. Dong, L. J. Richter, F. A. Escobedo, P. F. Nealey, S. N. Patel, C. K. Luscombe, *J. Mater. Chem.* **2021**, *9*, 21410.
- [28] X. Luo, H. Shen, K. Perera, D. T. Tran, B. W. Boudouris, J. Mei, *ACS Macro Lett.* **2021**, *10*, 1061.
- [29] J. Chen, W. Huang, D. Zheng, Z. Xie, X. Zhuang, D. Zhao, Y. Chen, N. Su, H. Chen, R. M. Pankow, Z. Gao, J. Yu, X. Guo, Y. Cheng, J. Strzalka, X. Yu, T. J. Marks, A. Facchetti, *Nat. Mater.* **2022**, *21*, 564.
- [30] T. C. H. Castillo, M. Moser, C. Cendra, P. D. Nayak, A. Salleo, I. McCulloch, S. Inal, *Chem. Mater.* **2022**, *34*, 6723.
- [31] C. B. Nielsen, A. Giovannitti, D.-T. Sbircea, E. Bandiello, M. R. Niazi, D. A. Hanifi, M. Sessolo, A. Amassian, G. G. Malliaras, J. Rivnay, I. McCulloch, *J. Am. Chem. Soc.* **2016**, *138*, 10252.
- [32] J. Mei, Y. Diau, A. L. Appleton, L. Fang, Z. Bao, *J. Am. Chem. Soc.* **2013**, *135*, 6724.
- [33] J. Mei, Z. Bao, *Chem. Mater.* **2014**, *26*, 604.
- [34] J. Xu, S. Wang, G. J. N. Wang, C. Zhu, S. Luo, L. Jin, X. Gu, S. Chen, V. R. Feig, J. W. F. To, S. Rondeau-Gagné, J. Park, B. C. Schroeder, C. Lu, J. Y. Oh, Y. Wang, Y. H. Kim, H. Yan, R. Sinclair, D. Zhou, G. Xue, B. Murmann, C. Linder, W. Cai, J. B. H. Tok, J. W. Chung, Z. Bao, *Science* **2017**, *355*, 59.
- [35] A. Giovannitti, R. B. Rashid, Q. Thiburce, B. D. Paulsen, C. Cendra, K. Thorley, D. Moia, J. T. Mefford, D. Hanifi, D. Weiyuan, M. Moser, A. Salleo, J. Nelson, I. McCulloch, J. Rivnay, *Adv. Mater.* **2020**, *32*, 1908047.
- [36] M. Moser, T. C. Hidalgo, J. Surgailis, J. Gladisch, S. Ghosh, R. Sheelamanthula, Q. Thiburce, A. Giovannitti, A. Salleo, N. Gasparini, A. Wadsworth, I. Zozoulenko, M. Berggren, E. Stavrinidou, S. Inal, I. McCulloch, *Adv. Mater.* **2020**, *32*, 2002748.
- [37] P. Li, J. Shi, Y. Lei, Z. Huang, T. Lei, *Nat. Commun.* **2022**, *13*, 5970.
- [38] H. Roh, C. Cunin, S. Samal, A. Gumyusenge, *MRS Commun.* **2022**, *12*, 565.
- [39] A. Khot, B. M. Savoie, *J. Polym. Sci.* **2022**, *60*, 610.
- [40] A. Giovannitti, I. P. Maria, D. Hanifi, M. J. Donahue, D. Bryant, K. J. Barth, B. E. Makdah, A. Savva, D. Moia, M. Zetek, P. R. F. Barnes, O. G. Reid, S. Inal, G. Rumbles, G. G. Malliaras, J. Nelson, J. Rivnay, I. McCulloch, *Chem. Mater.* **2018**, *30*, 2945.
- [41] T. M. McCormick, C. R. Bridges, E. I. Carrera, P. M. DiCarmine, G. L. Gibson, J. Hollinger, L. M. Kozycz, D. S. Seferos, *Macromolecules* **2013**, *46*, 3879.
- [42] S. Wood, J. Wade, M. Shahid, E. Collado-Fregoso, D. D. C. Bradley, J. R. Durrant, M. Heaney, J.-S. Kim, *Energy Environ. Sci.* **2015**, *8*, 3222.
- [43] H. Tran, S. Nikzad, J. A. Chiong, N. J. Schuster, A. E. Peña-Alcántara, V. R. Feig, Y.-Q. Zheng, Z. Bao, *Chem. Mater.* **2021**, *33*, 7465.
- [44] J. Rivnay, S. Inal, B. A. Collins, M. Sessolo, E. Stavrinidou, X. Strakosas, C. Tassone, D. M. Delongchamp, G. G. Malliaras, *Nat. Commun.* **2016**, *7*, 11287.
- [45] J. W. Onorato, C. K. Luscombe, *Mol. Syst. Des. Eng.* **2019**, *4*, 310.
- [46] D. T. Tran, A. Gumyusenge, X. Luo, M. Roders, Z. Yi, A. L. Ayzner, J. Mei, *ACS Appl. Polym. Mater.* **2020**, *2*, 91.
- [47] J. Li, Y. Zhao, H. S. Tan, Y. Guo, C.-A. Di, G. Yu, Y. Liu, M. Lin, S. H. Lim, Y. Zhou, H. Su, B. S. Ong, *Sci. Rep.* **2012**, *2*, 754.
- [48] E. L. Melenbrink, K. M. Hilby, M. A. Alkhadra, S. Samal, D. J. Lipomi, B. C. Thompson, *ACS Appl. Mater. Interfaces* **2018**, *10*, 32426.
- [49] M. Moser, A. Savva, K. Thorley, B. D. Paulsen, T. C. Hidalgo, D. Ohayon, H. Chen, A. Giovannitti, A. Marks, N. Gasparini, A. Wadsworth, J. Rivnay, S. Inal, I. McCulloch, *Angew. Chem., Int. Ed.* **2021**, *60*, 7777.
- [50] C. B. Nielsen, A. Giovannitti, D.-T. Sbircea, E. Bandiello, M. R. Niazi, D. A. Hanifi, M. Sessolo, A. Amassian, G. G. Malliaras, J. Rivnay, I. McCulloch, *J. Am. Chem. Soc.* **2016**, *138*, 10252.
- [51] M. Moser, L. R. Savagian, A. Savva, M. Matta, J. F. Ponder, T. C. Hidalgo, D. Ohayon, R. Hallani, M. Reissalali, A. Troisi, A. Wadsworth, J. R. Reynolds, S. Inal, I. McCulloch, *Chem. Mater.* **2020**, *32*, 6618.
- [52] L. R. Savagian, A. M. Österholm, J. F. Ponder, K. J. Barth, J. Rivnay, J. R. Reynolds, *Adv. Mater.* **2018**, *30*, 1804647.
- [53] M. Moser, J. Gladisch, S. Ghosh, T. C. Hidalgo, J. F. Ponder, R. Sheelamanthula, Q. Thiburce, N. Gasparini, A. Wadsworth, A. Salleo, S. Inal, M. Berggren, I. Zozoulenko, E. Stavrinidou, I. McCulloch, *Adv. Funct. Mater.* **2021**, *31*, 2100723.
- [54] S. E. Chen, L. Q. Flagg, J. W. Onorato, L. J. Richter, J. Guo, C. K. Luscombe, D. S. Ginger, *J. Mater. Chem.* **2022**, *10*, 10738.
- [55] T. J. Quill, G. LeCroy, A. Melianas, D. Rawlings, Q. Thiburce, R. Sheelamanthula, C. Cheng, Y. Tuchman, S. T. Keene,

- I. McCulloch, R. A. Segalman, M. L. Chabiny, A. Salleo, *Adv. Funct. Mater.* **2021**, *31*, 2104301.
- [56] J. Rivnay, P. Leleux, M. Ferro, M. Sessolo, A. Williamson, D. A. Koutsouras, D. Khodagholy, M. Ramuz, X. Strakosas, R. M. Owens, C. Benar, J.-M. Badier, C. Bernard, G. G. Malliaras, *Sci. Adv.* **2015**, *1*, e1400251.
- [57] M. Onen, N. Emond, B. Wang, D. Zhang, F. M. Ross, J. Li, B. Yildiz, J. A. del Alamo, *Science* **2022**, *377*, 539.
- [58] A. Sood, A. D. Poletayev, D. A. Cogswell, P. M. Csernica, J. T. Mefford, D. Fraggedakis, M. F. Toney, A. M. Lindenberg, M. Z. Bazant, W. C. Chueh, *Nat. Rev. Mater.* **2021**, *6*, 847.
- [59] S. J. Martin, P. D. Grimwood, R. G. M. Morris, *Annu. Rev. Neurosci.* **2000**, *23*, 649.
- [60] J. R. Whitlock, A. J. Heynen, M. G. Shuler, M. F. Bear, *Science* **2006**, *313*, 1093.
- [61] S. Pace, M. Ferrera, D. Convertino, G. Piccinini, M. Magnozzi, N. Mishra, S. Forti, F. Bisio, M. Canepa, F. Fabbri, C. Coletti, *J. Phys. Mater.* **2021**, *4*, 024002.
- [62] A. Melianas, T. J. Quill, G. LeCroy, Y. Tuchman, H. V. Loo, S. T. Keene, A. Giovannitti, H. R. Lee, I. P. Maria, I. McCulloch, A. Salleo, *Sci. Adv.* **2021**, *6*, eabb2958.
- [63] A. Gumyusenge, X. Zhao, Y. Zhao, J. Mei, *ACS Appl. Mater. Interfaces* **2018**, *10*, 4904.
- [64] Y. Zhao, C. Su, G. Shen, Z. Xie, W. Xiao, Y. Fu, S. Inal, Q. Wang, Y. Wang, W. Yue, I. McCulloch, D. He, *Adv. Funct. Mater.* **2022**, *32*, 2205744.